

Use of optical coherent detection for environmental sensing

Antonio Mecozzi,⁽¹⁾ Cristian Antonelli,⁽¹⁾

Mikael Mazur,⁽²⁾ Nicolas Fontaine,⁽²⁾ Haoshuo Chen,⁽²⁾ Lauren Dallachiesa,⁽²⁾ and Roland Ryf⁽²⁾

⁽¹⁾ Department of Physical and Chemical Sciences, University of L'Aquila, 67100 L'Aquila, Italy, antonio.mecozzi@univaq.it

⁽²⁾ Nokia Bell Labs, 600 Mountain Ave., Murray Hill, NJ 07974, USA

Abstract We discuss the use of the full transmission matrix extracted from a standard coherent receiver to improve the environmental sensing capabilities of optical fiber links.

Introduction

The cable of fiber optic coherent transmission systems is exposed to environmental perturbations, and the compensation of their effect requires that the receiver reconstructs the full transmission matrix of the link in real time. It has been recently shown^{[1],[2]} that the analysis of the temporal evolution of the state of polarization obtained by applying the fiber transmission matrix to a *fixed* input state may reveal the nature of the perturbations that affect the cable, turning the latter into a distributed sensor. However, by looking only at the evolution of a fixed input state, as was done in^{[1],[2]}, some of the information contained in the fiber transfer matrix is lost.

In this presentation we discuss the use of various quantities that can be extracted from measured transmission matrices, and compare their sensitivity to environmental perturbations. Our observations are based on data measured on deployed multi-core-fiber cables with nominally uncoupled cores.

Analysis

We start by considering the polar decomposition of the matrix describing a single-mode fiber-optic link $\mathbf{T} = \mathbf{U}\mathbf{A}$, where \mathbf{U} is a unitary matrix, and the intensity transmission matrix $\mathbf{T}^\dagger\mathbf{T} = \mathbf{A}^\dagger\mathbf{A}$ can be expressed as

$$\mathbf{T}^\dagger\mathbf{T} = g_0(\mathbf{I} + \vec{\Gamma} \cdot \vec{\sigma}), \quad (1)$$

where g_0 is the polarization-averaged intensity gain, $\vec{\Gamma}$ is a three-dimensional real-valued vector known as the polarization-dependent loss (PDL) vector,^[3] and $\vec{\sigma} = \sigma_1\hat{e}_1 + \sigma_2\hat{e}_2 + \sigma_3\hat{e}_3$ is the Pauli matrix vector.^[4] It is customary to quantify the fiber-link PDL by means of the power ratio in dB between the least and most attenuated polarization states, which can be seen to be^[3] $\rho = 10 \log[(1 - \Gamma)/(1 + \Gamma)]$, with $\Gamma = |\vec{\Gamma}|$.

The unitary matrix \mathbf{U} can be expressed as^[4]

$$\mathbf{U} = \exp\left(-i\frac{\varphi_0}{2}\mathbf{I} - i\frac{\vec{\varphi}}{2} \cdot \vec{\sigma}\right), \quad (2)$$

with $\vec{\varphi} = \varphi\hat{\varphi}$, where $\hat{\varphi}$ is the three-dimensional unit vector that defines the polarization rotation axes in Stokes space and φ is the rotation angle of the field polarization from the input to the output. The quantity φ_0 is the polarization-independent phase introduced by propagation. It should be noted that not only φ_0 is defined up to multiples of 2π , but also the expansion (2) is not unique, because of the identity $\mathbf{U} = (-1)^{m+n} \exp[-i(\varphi_0 + 2m\pi)\mathbf{I}/2 - i(\varphi + 2n\pi)\hat{\varphi} \cdot \vec{\sigma}/2]$, which holds for any pair of integers m and n . A change of sign of the Jones matrix does not affect the polarization state, so that besides the polarization averaged phase φ_0 , also φ is defined up to multiples of 2π . The values of φ_0 and $\vec{\varphi}$ can be extracted from \mathbf{U} through

$$\varphi_0 = i \text{trace}[\log(\mathbf{U})] = i \log[\det(\mathbf{U})], \quad (3)$$

$$\varphi_k = i \text{trace}[\log(\mathbf{U}) \sigma_k], \quad k = 1, 2, 3, \quad (4)$$

where $-2\pi < \varphi_k < 2\pi$ if one uses the principal value of the logarithm, that is, the logarithm with imaginary parts of the eigenvalues strictly between $-\pi$ and π .

Data analysis

The coherent receiver provides an estimate of the inverse channel transmission matrix by attempting to equalize the received signal. Assume, as is usually the case, that information is encoded in two independent signals transmitted over the x and y linear polarizations. After deskew, orthonormalization, and dispersion compensation, the digitized samples are processed by the constant modulus algorithm (CMA). The CMA seeks for a matrix \mathbf{C} that applied to the output field produces a constant modulus output

with a phase-modulated polarization-multiplexed input^[5] (QPSK in this work). This matrix is such that

$$\mathbf{CT} = \begin{pmatrix} e^{i\phi_1} & 0 \\ 0 & e^{i\phi_2} \end{pmatrix}. \quad (5)$$

Ideal channel reconstruction requires that $\phi_1 = \phi_2 = 0$ so that $\mathbf{C}^{-1} = \mathbf{T}$. A rotation of the two reconstructed constellations by ϕ_1 and ϕ_2 , however, does not affect the constant modulus of the output, so that these quantities, in general time dependent because of the frequency mismatch between transmit laser and local oscillator, are left undetermined by the CMA. The phases of the two constellations ϕ_1 and ϕ_2 are extracted at a successive stage, after frequency estimation and phase estimation of the two polarization multiplexed channels. The estimated transmission matrix \mathbf{T}' is the inverse of the equalization matrix, so that using $\mathbf{T}' = \mathbf{C}^{-1}$ and solving for \mathbf{T}' we obtain

$$\mathbf{T}' = \mathbf{T} \exp \left(-i \frac{\phi_1 + \phi_2}{2} \mathbf{I} - i \frac{\phi_1 - \phi_2}{2} \sigma_1 \right), \quad (6)$$

where we keep ϕ_1 and ϕ_2 non-zero to account for errors in frequency and phase estimation.

The polar decomposition of \mathbf{T}' can be accomplished by singular value decomposition applied to both sides of (6), $\mathbf{T}' = \mathbf{V}'_1 \mathbf{D}' \mathbf{V}'_2$, where \mathbf{D}' is a diagonal matrix with positive eigenvalues and \mathbf{V}'_1 and \mathbf{V}'_2 are unitary matrices. Then, being $\mathbf{T}' = (\mathbf{V}'_1 \mathbf{V}'_2) (\mathbf{V}'_2^{-1} \mathbf{D}' \mathbf{V}'_2) = \mathbf{U}' \mathbf{A}'$, we obtain $\mathbf{U}' = \mathbf{V}'_1 \mathbf{V}'_2$ and $\mathbf{A}' = \mathbf{V}'_2^{-1} \mathbf{D}' \mathbf{V}'_2$. The polar decomposition of both sides of Eq. (6) yields

$$\mathbf{U}' = \mathbf{U} \exp \left(-i \frac{\phi_1 + \phi_2}{2} \mathbf{I} - i \frac{\phi_1 - \phi_2}{2} \sigma_1 \right), \quad (7)$$

and, in Stokes spaces

$$\mathbf{R} = \exp(\vec{\varphi} \times), \quad (8)$$

$$\mathbf{R}' = \mathbf{R} \exp[(\phi_1 - \phi_2) \hat{e}_1 \times], \quad (9)$$

where \mathbf{R} and \mathbf{R}' are the link Mueller matrix and its estimate, respectively. Equations (8) and (9) show that only the x and y -polarized input states ($\hat{s} = \pm \hat{e}_1$) are not affected by the phase difference $\phi_1 - \phi_2$ and $\mathbf{R}' \hat{s} = \mathbf{R} \hat{s}$. Expressing

$$\mathbf{U}' = \exp \left(-i \frac{\varphi'_0}{2} \mathbf{I} - i \frac{\vec{\varphi}'}{2} \cdot \vec{\sigma} \right), \quad (10)$$

and $\mathbf{R}' = \exp(\vec{\varphi}' \times)$ we obtain a simple relation between the actual and estimated polarization averaged phase and rotation vectors

$$\varphi'_0 = \varphi_0 + \phi_1 + \phi_2, \quad (11)$$

$$\vec{\varphi}' \simeq \vec{\varphi} + (\phi_1 - \phi_2) \hat{e}_1, \quad (12)$$

the second being valid in the relevant regime where $\phi_1 \simeq \phi_2$ (as is the case in the absence of phase slips between the two constellations in the x and y signal polarization), and for small values of φ (as appropriate after removal of the average polarization rotation).

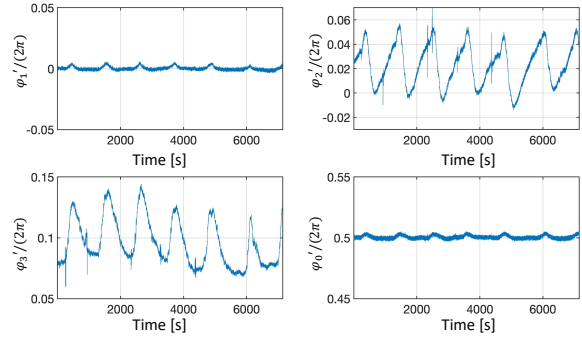


Fig. 1: Plot of the three components of $\vec{\varphi}'/(2\pi)$ and of the polarization-averaged phase $\varphi'_0/(2\pi)$ vs. time. The sampling rate has been reduced by a factor 1000 from the original, $T \simeq 524 \mu\text{s}$, by filtering and decimation.

The experimental values of \mathbf{T}' were measured in a recent real-time field trial^[6] by concatenating the cores of an uncoupled-core 4-core fiber deployed in the city of L'Aquila.^[7] The DSP of the receiver was based on an MSE estimation scheme, and was operating at a frequency $f_0 = 125$ MHz, with a baud rate $R = 1$ GBd (see^[6] for a detailed description of the experimental setup). The parameters of \mathbf{T}' were extracted with a downsampling factor of 2^{16} and hence the effective sampling time was $2^{16}/f_0 \simeq 524 \mu\text{s}$. After extracting the unitary part \mathbf{U}' by singular value decomposition, we have used Eqs. (3) and (4) to obtain the polarization-averaged phase φ'_0 and the components of the rotation vector $\vec{\varphi}'$.

Figure 1 shows the three components of $\vec{\varphi}'$ and the phase φ'_0 vs. time during a two-hour data acquisition. The figure shows that there is a strong correlation between φ'_1 and φ'_0 , which indicates that they are contributed mainly by ϕ_1 and ϕ_2 , as can be deduced from Eq. (11) and projecting Eq. (12) on \hat{e}_1 , thereby preventing the extraction of φ_0 and φ_1 . This implies that only two (out of four) parameters that are necessary to extract \mathbf{U} are immune to the phase fluctuations involved in ϕ_1 and ϕ_2 .

The second and third components of $\vec{\varphi}'$ presented in Fig. 1 show small perturbations that are most likely caused by events related to construction works taking place in the downtown area of L'Aquila along the fiber route. The same perturba-

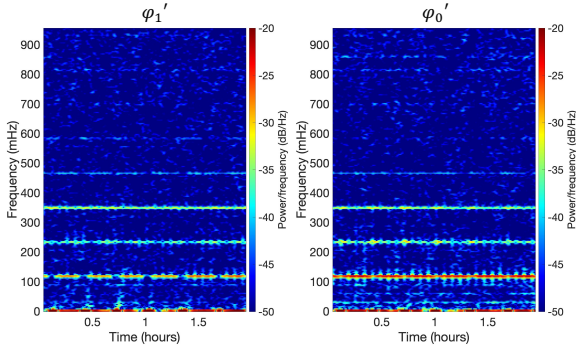


Fig. 2: Spectrogram of the first component of φ' and of the polarization-averaged phase φ'_0 .

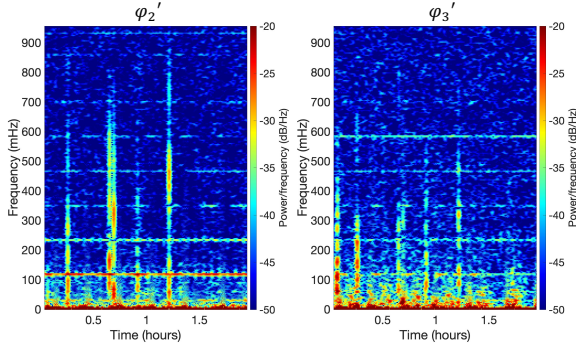


Fig. 3: Spectrogram of the second and third component of φ'

tions are not apparent in the first component of φ' and in the polarization-averaged phase φ'_0 , which are indeed much more stable. These features are confirmed by the spectrograms shown in Figs. 2 and 3. The vertical stripes in Fig. 3 correspond to the perturbations that appear in the temporal traces, and are not present in the spectrograms of Fig. 2. The higher stability of φ'_0 and φ'_1 , compared to φ'_2 and φ'_3 , can be explained by recalling that they depend mainly on phases ϕ_1 and ϕ_2 , which are determined by means of frequency locking and phase recovery on the output of the CMA algorithm. The phase recovery algorithm acts to compensate for the phase and frequency noise of the transmit and local oscillator lasers, and of course the perturbations induced by the construction works adds to those and are compensated as well. The other two components φ'_2 and φ'_3 are sensitive to the perturbations because their extraction does not depend on the phase recovery algorithm.

The horizontal lines that occur at frequencies that are multiples of $f = 117.5$ mHz are determined by the periodicity of the pseudo-random bit sequences (PRBSs) used in the measurement and the DSP readout frequency. Specifically, a PRBS with $(2^{23} - 1)$ bits was used for the load and an independent PRBS with $(2^7 - 1)$ bits was used for the header. For the used baud rate $R = 1$ GBd, the modulated signal was periodic with pe-

riod $T_R = N_p/R$ with $N_p = (2^{23} - 1)(2^7 - 1)$ (independent of the number of bits per symbol of the transmitted QAM constellations, as a result of the fact that N_p is an odd number hence not a multiple of any power of 2). The DSP readout frequency $f_0 = 125$ MHz was 8 times smaller than R , and therefore, being N_p not a multiple of 8, the *sampled* received signal was periodic with a period 8 times larger, $T_s = N_p/f_0$. This is consistent with the appearance of resonances at $f' = f_0/N_p = 117.3$ mHz. Being the observation window $T \simeq 7148$ s, $f' \simeq f$ within the temporal resolution of the measurement, $1/T \simeq 0.14$ mHz.

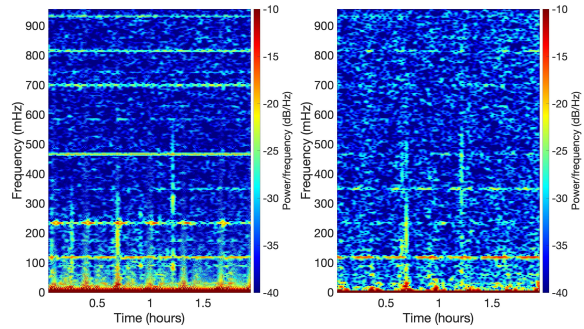


Fig. 4: Left panel, spectrogram of the polarization averaged gain. Right panel, spectrogram of the PDL in dB.

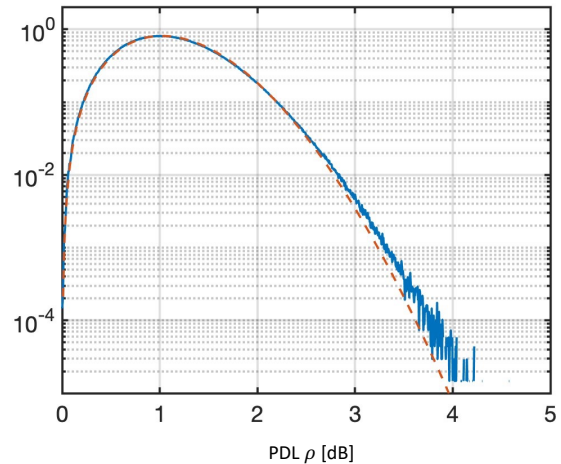


Fig. 5: Plot of the distribution of the PDL in dB, together with a Maxwellian distribution with the same average.

Vertical and horizontal lines appear also in the spectrograms of the polarization-averaged gain and the PDL in dB shown in Fig. 4. This is because in a fiber with random birefringence PDL and the polarization-averaged gain are coupled to polarization if the PDL is distributed along the line^[3], and hence PDL and gain are expected to show similar spectral features as polarization. Figure 5 shows the probability density function of the PDL in dB and its Maxwellian fit. The good agreement between the two may be an indication of the fact that the PDL is sufficiently distributed along the link.

Acknowledgements

The work of A. Mecozzi and C. Antonelli was supported in part by the Italian Government, in part by the project Innovating City Planning through Information and Communication Technologies (INCIPICT), and in part by the PRIN 2017 project Fiber Infrastructure for Research on Space-Division Multiplexed Transmission (FIRST).

References

- [1] Z. Zhan, M. Cantono, V. Kamalov, *et al.*, "Optical polarization-based seismic and water wave sensing on transoceanic cables", *Science*, vol. 371, no. 6532, pp. 931–936, 2021, ISSN: 0036-8075. DOI: 10.1126/science.abe6648. eprint: <https://science.sciencemag.org/content/371/6532/931.full.pdf>. [Online]. Available: <https://science.sciencemag.org/content/371/6532/931>.
- [2] A. Mecozzi, M. Cantono, J. C. Castellanos, V. Kamalov, R. Muller, and Z. Zhan, "Polarization sensing using submarine optical cables", *Optica*, vol. 8, no. 6, pp. 788–795, Jun. 2021. DOI: 10.1364/OPTICA.424307. [Online]. Available: <http://www.osapublishing.org/optica/abstract.cfm?URI=optica-8-6-788>.
- [3] A. Mecozzi and M. Shtaf, "Signal-to-noise-ratio degradation caused by polarization-dependent loss and the effect of dynamic gain equalization", *J. Lightwave Technol.*, vol. 22, no. 8, p. 1856, Aug. 2004. [Online]. Available: <http://opg.optica.org/jlt/abstract.cfm?URI=jlt-22-8-1856>.
- [4] J. P. Gordon and H. Kogelnik, "PMD fundamentals: Polarization mode dispersion in optical fibers", *Proceedings of the National Academy of Sciences*, vol. 97, no. 9, pp. 4541–4550, 2000, ISSN: 0027-8424. DOI: 10.1073/pnas.97.9.4541. eprint: <https://www.pnas.org/content/97/9/4541.full.pdf>. [Online]. Available: <https://www.pnas.org/content/97/9/4541>.
- [5] S. J. Savory, "Digital coherent optical receivers: Algorithms and subsystems", *IEEE Journal of Selected Topics in Quantum Electronics*, vol. 16, no. 5, pp. 1164–1179, 2010. DOI: 10.1109/JSTQE.2010.2044751.
- [6] M. Mazur, R. Ryf, N. K. Fontaine, *et al.*, "Real-time MIMO transmission over field-deployed coupled-core multi-core fibers", in *Optical Fiber Communication Conference (OFC) 2022*, Optica Publishing Group, 2022, Th4B.8. DOI: 10.1364/OFC.2022.Th4B.8. [Online]. Available: <http://opg.optica.org/abstract.cfm?URI=OFC-2022-Th4B.8>.
- [7] T. Hayashi, T. Nagashima, T. Nakanishi, *et al.*, "Field-deployed multi-core fiber testbed", in *2019 24th Opto-Electronics and Communications Conference (OECC) and 2019 International Conference on Photonics in Switching and Computing (PSC)*, 2019, pp. 1–3. DOI: 10.23919/PS.2019.8818058.